PHYSICAL REVIEW B **91**, 205420 (2015)

# Magnetic thermal switch for heat management at the nanoscale

Riccardo Bosisio,[1,2,*] Stefano Valentini,[3] Francesco Mazza,[3] Giuliano Benenti,[4,5]
Rosario Fazio,[3] Vittorio Giovannetti,[3] and Fabio Taddei[2]
[1]*SPIN-CNR, Via Dodecaneso 33, 16146 Genova, Italy*
[2]*NEST, Istituto Nanoscienze-CNR and Scuola Normale Superiore, I-56126 Pisa, Italy*
[3]*NEST, Scuola Normale Superiore, Istituto Nanoscienze-CNR, I-56126 Pisa, Italy*
[4]*Center for Nonlinear and Complex Systems, Università degli Studi dell'Insubria, via Valleggio 11, 22100 Como, Italy*
[5]*Istituto Nazionale di Fisica Nucleare, Sezione di Milano, via Celoria 16, 20133 Milano, Italy*
(Received 1 April 2015; revised manuscript received 24 April 2015; published 14 May 2015)

In a multiterminal setup, when time-reversal symmetry is broken by a magnetic field, the heat flows can be managed by designing a device with programmable Boolean behavior. We show that such a device can be used to implement operations, such as on/off switching, reversal, selected splitting, and swap of the heat currents. For each feature, the switching from one working condition to the other is obtained by inverting the magnetic field. This offers interesting opportunities for conceiving a programmable setup, whose operation is controlled by an external parameter (the magnetic field) without need to alter voltage and thermal biases applied to the system. Our results, generic within the framework of linear response, are illustrated by means of a three-terminal electronic interferometer model.

DOI: 10.1103/PhysRevB.91.205420 PACS number(s): 72.20.Pa, 73.23.−b, 84.60.−h

## I. INTRODUCTION

Heat management at the nanoscale is nowadays one of the leading research topics in many different scientific areas, including refrigeration and thermometry [1], coherent caloritronics [2], thermoelectric energy conversion [3–9], and information processing by utilizing phonons [10]. The overheating of microprocessor components is currently the most limiting factor in the development of information technology [11], which motivates the concern in finding alternative ways to control and evacuate heat in such devices. Theoretical works led to the possibility of controlling the heat currents and devise heat diodes [12] and transistors [13]. First experimental implementations exploiting phononic [14–16], electronic [17–19], or photonic [20] thermal currents were also reported.

It has been shown that the presence of a magnetic field breaking time reversibility could in principle enhance the efficiency of thermoelectric devices [21–25]. Interestingly a magnetic field allows for the simultaneous presence of reversible and irreversible heat currents [26,27]. Indeed, in a generic multiterminal setup, we can split the heat current $J_k^Q$, flowing from the $k$th terminal to the system, into the sum of a reversible and an irreversible part, $J_k^Q = J_k^{Q(r)} + J_k^{Q(i)}$. Although the reversible component changes sign by reversing the magnetic field $\mathbf{B}$, the irreversible component is invariant under the inversion $\mathbf{B} \to -\mathbf{B}$. Within the linear-response regime, it can be shown [26,27] that only the irreversible part of the current contributes to the entropy production. On the other hand the reversible part vanishes for $\mathbf{B} = 0$, whereas for $\mathbf{B} \neq 0$ it becomes arbitrarily large, giving rise, among other things, to the possibility of dissipationless transport, i.e., to a thermal machine operating at the Carnot efficiency with finite power output [23].

In this paper we take advantage of the presence of reversible components of the heat currents to propose a magnetic thermal switch, a Boolean setup which allows the control of heat flow by making use of an external magnetic field as a selector of the working configuration. For a generic multiterminal device operating in the linear-response regime, we show that by properly tuning the voltage biases we can access a broad spectrum of possible operating conditions, each of these being defined in terms of the behavior of the heat currents flowing through the system. Namely, it is possible to design a *programmable* device for the management of heat flows, allowing several Boolean features, such as selected splitting, on/off switching, reversal, and swap of the heat currents. For each feature, the magnetic field acts as a knob selecting one of the two possible working conditions without the need to modify the reservoirs parameters (temperatures and electrochemical potentials): The switching from one working condition to the other is obtained by inverting the direction of the magnetic field.

A significant advantage of our approach is the absence of temperature constraints: As long as the system operates in linear response, our results hold. In particular, the method we present is valid whether the heat is transported by electrons, by phonons, or by both. Thus, remarkably, it constitutes a possible way of manipulating phononic heat currents using a magnetic field. From a practical point of view, the implementation of our theoretical results would require a full characterization of the Onsager matrix, the major difficulty being the measurement of the heat currents at the nanoscale, a challenge for which, however, important advances have been recently reported [28,29]. Moreover, assuming the system in contact with regions having finite thermal capacitance rather than with ideally infinite reservoirs, the magnetic-field switching could be used to control the temperatures of such regions, allowing for instance the initialization of qubit states or the implementation of thermal logic gate operations [10]. We finally remark that there exists, in the literature, a variety of works on interferometer-based systems which, under broken time-reversal symmetry, would constitute natural physical realizations of our model (see, for instance, Refs. [9,21,22,30–37]).

*Corresponding author: riccardo.bosisio@nano.cnr.it

 

The paper is structured as follows: In Sec. II we describe the theoretical implementation of the magnetic thermal switch for a general multiterminal setup. Then in Sec. III we present some results of numerical simulations using an interferometer in contact with three reservoirs as a toy model. Finally, we draw our conclusions in Sec. IV. Details of the calculations and the derivation of the scattering matrix of the interferometer are gathered in the Appendices.

## II. MAGNETIC THERMAL SWITCH

In this section we discuss how a magnetic thermal switch can be implemented in a general multiterminal setup. Let us consider a generic system in contact with $n$ reservoirs at temperatures $T_k = T + \Delta T_k$ and electrochemical potentials $\mu_k = \mu + \Delta\mu_k$, $T$ and $\mu$ being some equilibrium (reference) values. Let $\mathbf{J}_k = (J_k^N, J_k^Q)$ denote the particle ($J_k^N$) and heat ($J_k^Q$) currents from the $k$th terminal to the system and $\mathbf{X}_k = (X_k^\mu, X_k^T) = (\Delta\mu_k/T, \Delta T_k/T^2)$ the conjugated affinities [38]. Within linear irreversible thermodynamics, the fluxes $\mathbf{J} = (\mathbf{J}_1, \ldots, \mathbf{J}_{n-1})^T$ and the conjugated affinities $\mathbf{X} = (\mathbf{X}_1, \ldots, \mathbf{X}_{n-1})^T$ are related as follows:

$$\mathbf{J} = \mathbf{L}\mathbf{X}, \tag{1}$$

where $\mathbf{L}$ is the Onsager matrix of kinetic coefficients [38] of dimension $2(n-1) \times 2(n-1)$. Note that, due to the constraints of particle and energy conservation, we can determine $\mathbf{J}_n$ from the fluxes $\mathbf{J}_1, \ldots, \mathbf{J}_{n-1}$. Moreover, we set the $n$th reservoir as the reference one, with temperature $T$ and electrochemical potential $\mu$. In the presence of a magnetic field $\mathbf{B}$, time-reversal symmetry is broken, and the Onsager matrix $\mathbf{L}$ in general is not symmetric [23,24,38]. The currents can be separated into *reversible* components (which change sign by reversing $\mathbf{B} \to -\mathbf{B}$) and *irreversible* components (which are invariant with respect to the inversion $\mathbf{B} \to -\mathbf{B}$) [26,27],

$$\mathbf{J}^{(r)} \equiv \frac{\mathbf{L}(\mathbf{B}) - \mathbf{L}^T(\mathbf{B})}{2}\mathbf{X}, \qquad \mathbf{J}^{(i)} \equiv \frac{\mathbf{L}(\mathbf{B}) + \mathbf{L}^T(\mathbf{B})}{2}\mathbf{X}. \tag{2}$$

By virtue of the Onsager-Casimir relations $L_{ij}(-\mathbf{B}) = L_{ji}(\mathbf{B})$ [38], these currents have the properties that $\mathbf{J}^{(r)}(\mathbf{B}) = -\mathbf{J}^{(r)}(-\mathbf{B})$ and $\mathbf{J}^{(i)}(\mathbf{B}) = \mathbf{J}^{(i)}(-\mathbf{B})$. In general these properties imply that $\mathbf{J}(\mathbf{B}) = \mathbf{J}^{(r)}(\mathbf{B}) + \mathbf{J}^{(i)}(\mathbf{B}) \neq \mathbf{J}^{(r)}(-\mathbf{B}) + \mathbf{J}^{(i)}(-\mathbf{B}) = \mathbf{J}(-\mathbf{B})$.

The idea of the present proposal is to set proper working conditions that enforce a given target functional dependence between the thermal currents evaluated at $\mathbf{B}$ and $-\mathbf{B}$. For instance we may ask the current $J_k^Q(\mathbf{B})$ we get at the $k$th contact to be equal to twice the current $J_{k'}^Q(-\mathbf{B})$ one would get at the $k'$th contact when flipping the orientation of the magnetic field. More generally, given a subset $K$ of the $n$ terminals of the system, we will write our target functional dependence in the form of a linear constraint,

$$J_k^Q(-\mathbf{B}) = \sum_{k'=1}^{n-1} x_{kk'}^{(\mathrm{target})} J_{k'}^Q(\mathbf{B}), \qquad \forall\, k \in K, \tag{3}$$

where $x_{kk'}^{(\mathrm{target})}$ is an assigned $(n_0 - 1) \times (n-1)$ real matrix with $n_0 \leqslant n-1$ being the number of elements of $K$. This allows us to define different Boolean working conditions which, while maintaining constant all the other system parameters, can be activated by simply operating on the relative orientation of the device with respect to the external magnetic field: Special instances of these devices are explicitly discussed in the following subsections.

Once the Onsager matrix $L_{ij}(\mathbf{B})$ and the coefficients $x_{kk'}^{(\mathrm{target})}$ are given, one can satisfy Eq. (3) by properly tuning the components of the affinity vector $\mathbf{X}$. As a matter of fact, since the conditions (3) are at most $n-1$ and the total number of the affinity parameters is $2(n-1)$, we can fulfill the former by only using half of the latter. In what follows we exploit this freedom to fix the values of the thermal affinity components $\{X_k^T\}$'s on each of the reservoirs [39], whereas using the $\{X_k^\mu\}$'s to enforce the constraint (3). When $n_0 = n-1$, i.e., if we impose constraints on the $J_k^Q(-\mathbf{B})$'s of all the terminals of the system, the procedure has the limitation of making the device operate *only* for certain precise values of the currents flowing from each $k$th reservoir. Indeed, imposing $n-1$ relations of the form of Eq. (3) univocally determines all the $\{X_k^\mu\}$'s and hence, assuming fixed temperatures, all the $J_k^Q(\pm\mathbf{B})$'s. This limitation is naturally overcome when $n_0$ is strictly smaller than $n-1$. For instance, one may choose to impose only one condition (i.e., $n_0 = 1$) in order to leave all but one of the $\{X_k^\mu\}$'s unspecified. In particular, we could solve for $X_1^\mu$ to obtain

$$X_1^\mu = a_2 X_2^\mu + \cdots + a_{n-1} X_{n-1}^\mu + f\left(X_1^T, \ldots, X_{n-1}^T\right), \tag{4}$$

where $a_k$ are some functions of the Onsager matrix elements $L_{ij}$, whereas $f(X_1^T, \ldots, X_{n-1}^T)$ depends on the temperatures and on $L_{ij}$. Setting $X_1^\mu = \text{const}$, Eq. (4) defines a $(n-2)$-dimensional hypersurface in the space spanned by $(X_2^\mu, \ldots, X_{n-1}^\mu)$. Assuming constant temperatures, varying the electrochemical potentials along this surface allows changing the values of the heat currents, without compromising the working operation of the device. In this way, we use the extra degrees of freedom given by the reservoirs with free electrochemical potential to widen the operational range of the device to many values of the heat currents [40].

### A. Heat current multiplier

In general, we may design a system in which the heat current in the $k$th terminal becomes a fraction or a multiple of the original value when the magnetic field is reversed, which corresponds to having a diagonal matrix $x_{kk'}^{(\mathrm{target})} = \delta_{kk'} x_k$ in Eq. (3): $J_k^Q(-\mathbf{B}) = x_k J_k^Q(\mathbf{B})$. Specifying a value for $x_k$ makes the system operate as a Boolean *heat current multiplier* in which the two (Boolean) configurations correspond to an upward or a downward magnetic field. A schematic of such an operation for a three-terminal device is shown in Fig. 1(a).

#### 1. On/off switch

Let us consider the specific case of a heat current multiplier in which $x_k = 0$: The device behaves as an *on/off switch for the kth terminal*, which means $J_k^Q(-\mathbf{B}) = J_k^{Q(r)}(-\mathbf{B}) + J_k^{Q(i)}(-\mathbf{B}) = 0$, whereas $J_k^Q(\mathbf{B}) = J_k^{Q(r)}(\mathbf{B}) + J_k^{Q(i)}(\mathbf{B}) \neq 0$. It is then clear that $J_k^{Q(i)}(\mathbf{B})$ and $J_k^{Q(r)}(\mathbf{B})$ have the same magnitude and the same sign and add up giving a finite current, whereas the two terms cancel out upon magnetic-field reversal, resulting in a *vanishing* heat current. This principle could be

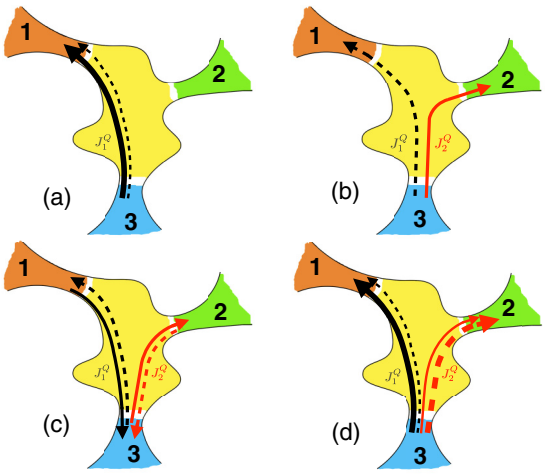


FIG. 1. (Color online) Examples of operational principles for a three-terminal magnetic thermal switch. The different panels illustrate the heat current (a) multiplier, (b) selector, (c) reversal, and (d) swap configurations, respectively. The working operation is selected by choosing either $+\mathbf{B}$ or $-\mathbf{B}$. Solid (dashed) lines correspond to $J^Q(+\mathbf{B})[J^Q(-\mathbf{B})]$, whereas black (red) lines refer to currents flowing from terminal 1(2). Notice that in panel (a) lines of different thicknesses have been used to emphasize the increase/decrease of the heat currents magnitude before and after the magnetic-field reversal.

used, for instance, to implement a $n$-terminal *selector for the heat path* in which an upward magnetic field allows the flow of heat through $l$ channels while blocking it into the remaining $(n-l)$ ones and vice versa by reversing $\mathbf{B} \to -\mathbf{B}$. A schematic of such an operation for a three-terminal device is shown in Fig. 1(b).

#### 2. *Fully reversible heat*

Another interesting configuration is obtained by setting $x_k = -1$ in which case the heat current is *fully reversible* [41] ($J_k^{Q(i)} = 0$). As an application, one could conceive a device in which the heat currents flowing through some (or all) the channels simultaneously flip their sign upon reversing the magnetic field. This, among other things, would offer the possibility of switching from a "refrigerator" mode for a specific reservoir to a "thermal engine" one by simply using the external magnetic field without needing to modify the gradients in the reservoirs. A schematic of such an operation for a three-terminal device is shown in Fig. 1(c). Note that, by analogous considerations, $x_k = 1$ corresponds to the case of *fully irreversible* heat currents, which is however much less interesting because in this situation reversing the magnetic field has no effect.

### B. Heat current swap

The matrix $x_{kk'}^{(\mathrm{target})}$ which defines our target (3) does not need to be diagonal. For instance let us consider the case where $x_{kk'}^{(\mathrm{target})} = x_{k'k}^{(\mathrm{target})} = 1$ and $x_{kk}^{(\mathrm{target})} = x_{k'k'}^{(\mathrm{target})} = 0$, which implements a *heat current swap* between reservoirs $k$ and $k'$. This configuration couples heat currents flowing from different terminals, whereas in the previous ones the conditions were imposed on each single reservoir independently. Such a choice for $x_{kk'}^{(\mathrm{target})}$ results in having $J_k^Q(\mathbf{B}) = J_{k'}^Q(-\mathbf{B})$ and $J_{k'}^Q(\mathbf{B}) = J_k^Q(-\mathbf{B})$, i.e., the two heat currents are swapped by reversing the magnetic field, as pictorially shown in Fig. 1(d) for a three-terminal case. Besides, we notice that in this situation the reversible and irreversible components of the heat currents satisfy the conditions: $J_k^{Q(i)} = J_{k'}^{Q(i)}$ and $J_k^{Q(r)} = -J_{k'}^{Q(r)}$.

It is worth stressing that in a generic multiterminal setup different working conditions can coexist: For instance, some channels can be configured as heat current selectors, whereas others may operate as multipliers, make heat reversal, or swap.

## III. SIMPLE MODEL

In order to illustrate the effects discussed in the previous section, we study a simple noninteracting model consisting of a three-terminal interferometer sketched in Fig. 2. We assume for simplicity low temperatures so that electrons are the only heat carriers. Under these conditions, the electronic transport through the device is coherent, which allows us to follow a scattering approach [42]. The system consists of an interference loop, for example, made by two clean wires and connected to three electronic reservoirs with temperatures $T_k$ and electrochemical potentials $\mu_k$ ($k = 1,2,3$). A magnetic field $\mathbf{B}$ orthogonal to the interferometer plane generates a magnetic flux $\Phi$ piercing the loop, which will be the relevant parameter in the following discussion (from here on, we will assume $\Phi$ to be expressed in units of $h/2e$). A scattering region $S_s$ is inserted into channel 1, having the effect of breaking the particle-hole symmetry $E \to -E$ (having set $\mu = 0$ as the reference zero energy) in order to have finite nondiagonal Onsager coefficients. The specific choice of such scatterer is not important for the present discussion as it does not alter the results at a qualitative level. Further details on the computation of the scattering matrix of this system are given in Appendix A. Following the notation of the previous section, we set reservoir 3 as the reference one ($\{\mu_3, T_3\} \equiv \{\mu, T\}$), and we express the particle and heat currents flowing from the other two reservoirs

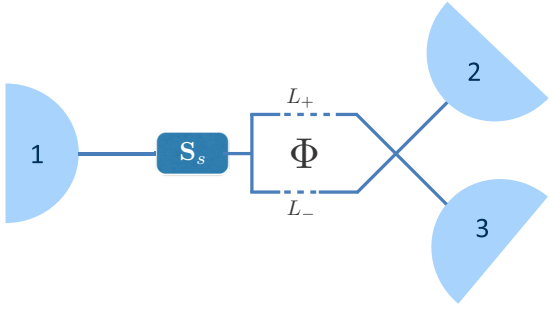


FIG. 2. (Color online) Sketch of the three-terminal magnetic thermal switch studied numerically: an electronic interferometer, pierced by a magnetic flux $\Phi$ and in contact with three reservoirs at different temperatures $T_k$ and electrochemical potentials $\mu_k$ ($k = 1,2,3$). The scattering region $S_s$ inside channel 1 breaks the particle-hole symmetry. $L_+$ and $L_-$ are the interference paths and must be different in order to observe interference at the end of the device.

via the following $4 \times 4$ linear system [43]:

$$\begin{pmatrix} J_1^N \\ J_1^Q \\ J_2^N \\ J_2^Q \end{pmatrix} = \begin{pmatrix} L_{11} & L_{12} & L_{13} & L_{14} \\ L_{21} & L_{22} & L_{23} & L_{24} \\ L_{31} & L_{32} & L_{33} & L_{34} \\ L_{41} & L_{42} & L_{43} & L_{44} \end{pmatrix} \begin{pmatrix} X_1^\mu \\ X_1^T \\ X_2^\mu \\ X_2^T \end{pmatrix}. \tag{5}$$

The coefficients $L_{ij}$ are functions of the magnetic flux $\Phi$ and therefore of the applied magnetic field $\mathbf{B}$. Their explicit expressions are given by Eqs. (B1), derived in Appendix B. The reversible ($r$) and irreversible ($i$) components of the heat currents $J_1^Q$ and $J_2^Q$ are [44] as follows:

$$\begin{aligned} J_1^{Q(r)} &= \frac{L_{23}-L_{32}}{2} X_2^\mu + \frac{L_{24}-L_{42}}{2} X_2^T, \\ J_1^{Q(i)} &= L_{21} X_1^\mu + L_{22} X_1^T + \frac{L_{23}+L_{32}}{2} X_2^\mu + \frac{L_{24}+L_{42}}{2} X_2^T, \\ J_2^{Q(r)} &= \frac{L_{41}-L_{14}}{2} X_1^\mu + \frac{L_{42}-L_{24}}{2} X_1^T, \\ J_2^{Q(i)} &= \frac{L_{41}+L_{14}}{2} X_1^\mu + \frac{L_{42}+L_{24}}{2} X_1^T + L_{43} X_2^\mu + L_{44} X_2^T. \end{aligned} \tag{6}$$

Once the $L_{ij}$ coefficients *for a given magnetic flux* $\Phi_0$ are calculated, for fixed $X_{1,2}^T$ different Boolean working conditions can be achieved by tuning the electrochemical potentials (and hence $X_{1,2}^\mu$) in order to impose Eq. (3) in both channels 1 and 2. Then, the switch is realized by reversing the magnetic field $\mathbf{B} \to -\mathbf{B}$, and hence the flux $\Phi_0 \to -\Phi_0$. In order to illustrate the effects outlined in the previous section, we focus here below on the same four working conditions by properly choosing the values of $x_{kk'}^{(\text{target})}$ appearing in Eq. (3). The numerical results are summarized in Fig. 3: Notice that both the heat (symbols) and the particle (dashed lines) currents are shown to stress that they are not constrained to follow the same behaviors.

(a) *Heat current multiplier* $(x_1,x_2) = (1/2,2)$. In this case the heat currents satisfy

$$\begin{aligned} J_1^Q(-\mathbf{B}) &= \frac{1}{2} J_1^Q(+\mathbf{B}), \\ J_2^Q(-\mathbf{B}) &= 2 J_2^Q(+\mathbf{B}), \end{aligned} \tag{7}$$

that is, by reversing the magnetic field $J_1^Q$ is halved whereas $J_2^Q$ is doubled. Under these conditions, by using Eqs. (3) and (7), it is straightforward to see that the reversible and irreversible components of the heat currents are related via $J_1^{Q(i)}(\mathbf{B}) = 3 J_1^{Q(r)}(\mathbf{B})$ and $J_2^{Q(i)}(\mathbf{B}) = -3 J_2^{Q(r)}(\mathbf{B})$. The behavior of the heat currents flowing through the interferometer as a function of the magnetic flux in this configuration is shown in Fig. 3(a) for the interferometer described above.

(b) *Heat path selector* $(x_1,1/x_2) = (0,0)$. In this case the heat currents satisfy $J_1^Q(\mathbf{B}) \neq 0$, $J_2^Q(\mathbf{B}) = 0$ and $J_1^Q(-\mathbf{B}) = 0$, $J_2^Q(-\mathbf{B}) \neq 0$, i.e., for an upward magnetic field, heat transfer is allowed between the system and reservoir 1 while being blocked between the system and reservoir 2. This situation is reversed by changing $\mathbf{B} \to -\mathbf{B}$ ($\Phi_0 \to -\Phi_0$). Furthermore, according to Eqs. (3) and (7), the reversible and irreversible components of the heat currents are related via $J_1^{Q(i)}(\mathbf{B}) = J_1^{Q(r)}(\mathbf{B})$ and $J_2^{Q(i)}(\mathbf{B}) = -J_2^{Q(r)}(\mathbf{B})$. The behavior of $J_1^Q$ and $J_2^Q$ is shown in Fig. 3(b).

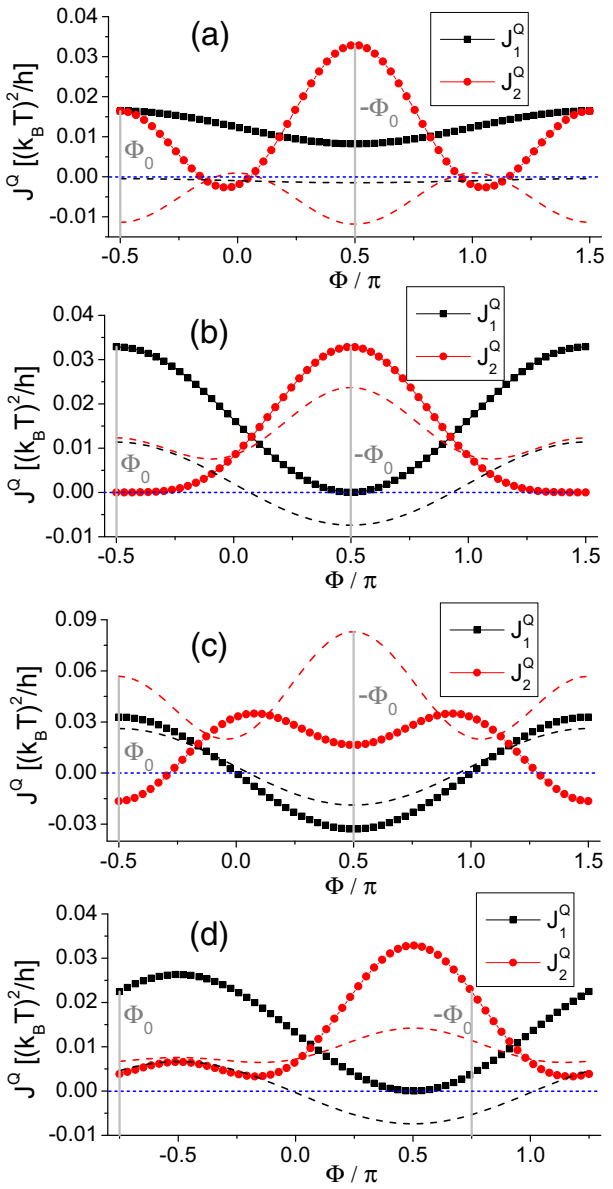


FIG. 3. (Color online) Working operations of the three-terminal magnetic thermal switch discussed in the text. The heat currents through channels 1 (black squares) and 2 (red circles) are shown as a function of the magnetic flux $\Phi$ enclosed in the interferometer. For completeness, the particle currents (black and red dashed lines) are also shown to emphasize that they do not follow the same behaviors as the heat currents. (a) *Heat current multiplier*: By reversing $\Phi$ from $\Phi_0 = -\pi/2$ to $-\Phi_0 = +\pi/2$, $J_1^Q$ is halved whereas $J_2^Q$ is doubled. (b) *Heat path selector*: For $\Phi_0 = -\pi/2$, $J_1^Q$ is finite whereas $J_2^Q$ is blocked. The situation is opposite by reversing $\Phi$ to $-\Phi_0$. (c) *Heat current reversal*: By reversing $\Phi$ from $-\pi/2$ to $+\pi/2$, the signs of both $J_1^Q$ and $J_2^Q$ flip. (d) *Heat current swap*: By reversing $\Phi$ from $-3\pi/4$ to $+3\pi/4$, the values of $J_1^Q$ and $J_2^Q$ are interchanged. The parameters are $k_B T = 1$, $\mu = 0$, $X_1^T = 0.025$, $X_2^T = 0.01$ [except in (c), where $X_1^T = -0.005$ and $X_2^T = 0.005$] and the difference between the interference paths in the upper/lower interferometer arms is $\Delta(kL) \equiv k(L_+ - L_-) = \pi/2$. Dotted blue lines are guides to the eye at $J^Q = 0$, whereas gray lines highlight the magnetic flux values $\Phi = \pm\Phi_0$ selecting the two Boolean configurations.

(c) *Heat current reversal* $(x_1,x_2) = (-1,-1)$. In this case the heat currents are purely reversible, that is, $J_1^{Q(i)} = J_2^{Q(i)} = 0$. Reversing the magnetic flux through the interferometer makes them simultaneously change their sign. The behavior of $J_1^Q$ and $J_2^Q$ is shown in Fig. 3(c). Note that at $\Phi_0 = -\pi/2$ both $J_1^Q$ (black squares) and $J_1^N$ (black dashed line) are positive. This, together with the fact that $X_1^\mu > 0$ in this case, means that the system is acting as a *local refrigerator* [45] for reservoir 1, exploiting a positive $\Delta\mu_1$ to extract heat from a cold bath ($X_1^T < 0$). Conversely, at $\Phi = -\Phi_0 = \pi/2$, both $J_1^Q$ and $J_1^N$ have changed their signs: The system is now performing work driving particles against $\Delta\mu_1$, thus operating as a thermal engine. Notice that the same reasoning does not hold for reservoir 2 in which, upon reversing the magnetic flux, the sign of $J_2^Q$ flips whereas that of $J_2^N$ does not.

(d) *Heat current swap* $(x_{12},x_{21}) = (1,1)$. The heat currents satisfy $J_1^Q(\mathbf{B}) = J_2^Q(-\mathbf{B})$ and $J_2^Q(\mathbf{B}) = J_1^Q(-\mathbf{B})$, that is, the two heat currents are swapped by reversing the magnetic field. Furthermore, according to Eqs. (3) and (7), the reversible and irreversible components of the heat currents are related via $J_1^{Q(i)}(\mathbf{B}) = J_2^{Q(i)}(\mathbf{B})$ and $J_1^{Q(r)}(\mathbf{B}) = -J_2^{Q(r)}(\mathbf{B})$. The behavior of $J_1^Q$ and $J_2^Q$ is shown in Fig. 3(d).

## IV. CONCLUSIONS

In this article we have shown that a magnetic thermal switch can be implemented within the framework of linear response, taking advantage of the generic existence of reversible heat currents when time-reversal symmetry is broken. Such a device could allow the implementation of several Boolean features, such as on/off switching, reversal, selected splitting, and swap of the heat currents. For each feature, the switching from one working condition to the other is obtained by inverting the direction of an applied magnetic field. Quite interestingly, it is possible to change the operating mode of the device (from a power generator to a refrigerator) with respect to one of the reservoirs by inverting the external driving parameter, i.e., the magnetic field, at fixed electrochemical potentials and temperatures of the reservoirs.

A further advantage of our magnetic switch would arise in the perspective of conceiving a more complex programmable system made of (for instance) an array of $N$ simpler subsystems. These may be set up to operate in a variety of independent configurations but always defined in terms of conditions of the form Eq. (3). We could imagine designing an array of $N$ elements that are all initialized in the same state (say, for upward magnetic field $\mathbf{B}$) but that upon reversing $\mathbf{B} \to -\mathbf{B}$ go to (possibly all different) final states. We stress once more that acting on a *single* parameter—the magnetic field—would be enough to achieve this operation and to reinitialize them in a subsequent moment, if needed.

Note that, although we have illustrated the magnetic thermal switch for a low-temperature interferometer model with the heat carried by the electrons, the mechanism discussed in this paper is generic for any system with the time-reversal symmetry broken by a magnetic field. A magnetic thermal switch could be in principle implemented also when both fermionic and bosonic reservoirs are present. Indeed, as shown in Ref. [46] due to the electron-phonon coupling the Onsager kinetic coefficients connecting the phononic heat currents from the bosonic reservoirs to the affinities for the fermionic terminals, in general, are not even functions of the magnetic field. As a consequence, the phononic heat current generally exhibits a reversible component, and our theory can be applied.

## ACKNOWLEDGMENTS

Stimulating discussions with F. Giazotto are gratefully acknowledged. This work has been supported by Grant No. MIUR-FIRB2013—Project Coca (Grant No. RBFR1379UX), by the EU project "ThermiQ," by MIUR-PRIN "Collective quantum phenomena: from strongly correlated systems to quantum simulators," by the EU project COST Action Project No. MP1209 "Thermodynamics in the quantum regime," and by the by the EU project COST Action Project No. MP1201 "Nanoscale Superconductivity: Novel Functionalities through Optimized Confinement of Condensate and Fields".

## APPENDIX A: MODELING THE INTERFEROMETER

In this section we outline the procedure followed to compute the scattering matrix of our interferometric system. We start by considering an interferometer realized by connecting two four-arm beam splitters via two clean wires (see Fig. 4). For simplicity, we assume the beam splitters to be identical and symmetric, that means, each one is described by a scattering matrix of the form

$$S_{bs} = \begin{pmatrix} r_{11} & t_{12} & t_{13} & t_{14} \\ t_{21} & r_{22} & t_{23} & t_{24} \\ t_{31} & t_{32} & r_{33} & t_{34} \\ t_{41} & t_{42} & t_{43} & r_{44} \end{pmatrix} = \begin{pmatrix} 0 & 1/\sqrt{2} & 1/\sqrt{2} & 0 \\ 1/\sqrt{2} & 0 & 0 & 1/\sqrt{2} \\ 1/\sqrt{2} & 0 & 0 & -1/\sqrt{2} \\ 0 & 1/\sqrt{2} & -1/\sqrt{2} & 0 \end{pmatrix}. \quad \text{(A1)}$$

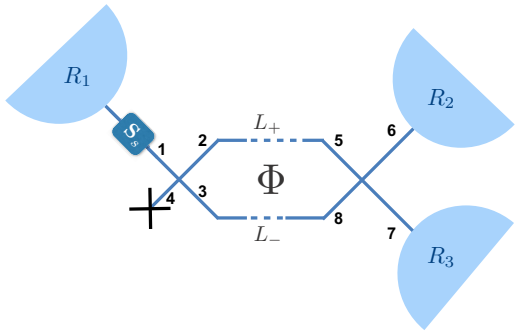


FIG. 4. (Color online) Sketch of the system used to model the interferometer discussed in Sec. III. Two identical four-arm beam splitters are connected via two clean electronic waveguides of lengths $L_+$ and $L_-$, forming an interference loop which is pierced by a magnetic flux $\Phi$. A scatterer $S_s$ is inserted into arm 1 in order to break the particle-hole symmetry. The numbers from 1 to 8 refer to the arms of the beam splitters and label the transmission and reflection amplitudes $t_{ij}$ and $r_{ij}$ (in particular, channel 4 is assumed to be totally reflective). The system is connected to three electronic reservoirs $R_1$, $R_2$, and $R_3$.

The matrix $S_{bs}$ describes a 50:50 beam splitter of electron waves for which all the reflection terms are zero and such that particles entering through one arm can be transmitted into two of the other three with equal probability one half. According to the notation of Fig. 4, we have to compose the scattering matrices of the two individual beam splitters with the free propagation phase terms associated with the two interference paths. These terms are products of both the geometric (Aharonov-Bohm) phase and the dynamical phase exponentials,

$$\begin{aligned} f_{25} &= f_g^+ f_d^+, \quad f_{38} = (f_g^-)^* f_d^-, \\ f_{52} &= (f_g^+)^* f_d^+, \quad f_{83} = f_g^- f_d^-, \end{aligned} \tag{A2}$$

where $f_g^+ f_g^- = \exp\{i\Phi\}$, $f_d^\pm = \exp\{ikL_\pm\}$, the $\pm$ signs denote the upper $(+)$ and lower $(-)$ interference arms of lengths $L_\pm$, the complex conjugation accounts for the electron traveling direction, $\Phi$ denotes the magnetic flux enclosed in the interferometer, and $k$ is the Fermi wave vector. For simplicity we neglect the energy dependence of the free propagations. The resulting scattering matrix describes the propagation among channels 1, 4, 6, and 7 and reads

$$S_i^{(1)} = \begin{pmatrix} 0 & 0 & t_{16} & t_{17} \\ 0 & 0 & t_{46} & t_{47} \\ t_{61} & t_{64} & 0 & 0 \\ t_{71} & t_{74} & 0 & 0 \end{pmatrix}, \tag{A3}$$

where the various coefficients $t_{pq}$ account for the different possible paths along which particles can travel from $p$ to $q$,

$$\begin{aligned} t_{16} &= t_{12} f_{25} t_{56} + t_{13} f_{38} t_{86}, \quad t_{17} = t_{12} f_{25} t_{57} + t_{13} f_{38} t_{87}, \\ t_{46} &= t_{42} f_{25} t_{56} + t_{43} f_{38} t_{86}, \quad t_{47} = t_{42} f_{25} t_{57} + t_{43} f_{38} t_{87}, \\ t_{61} &= t_{65} f_{52} t_{21} + t_{68} f_{83} t_{31}, \quad t_{71} = t_{75} f_{52} t_{21} + t_{78} f_{83} t_{31}, \\ t_{64} &= t_{65} f_{52} t_{24} + t_{68} f_{83} t_{34}, \quad t_{74} = t_{75} f_{52} t_{24} + t_{78} f_{83} t_{34}. \end{aligned} \tag{A4}$$

Now, since we are interested in a three-terminal configuration, we impose that one of the channels (say, channel 4) behaves as a purely reflective mirror characterized by a reflection amplitude $r = -1$. The interferometer scattering matrix thus reduces to a $3 \times 3$ matrix,

$$S_i^{(2)} = \begin{pmatrix} r'_{11} & t'_{16} & t'_{17} \\ t'_{61} & r'_{66} & t'_{67} \\ t'_{71} & t'_{76} & r'_{77} \end{pmatrix} = \begin{pmatrix} 0 & t_{16} & t_{17} \\ t_{61} & t_{64} r t_{46} & t_{64} r t_{47} \\ t_{71} & t_{74} r t_{46} & t_{74} r t_{47} \end{pmatrix}. \tag{A5}$$

Finally, in order to break the particle-hole symmetry, we insert in channel 1 an energy-dependent scattering region, described by a scattering matrix,

$$S_s = \begin{pmatrix} \rho & i\tau \\ i\tau & \rho \end{pmatrix}, \tag{A6}$$

where $\rho, \tau \geqslant 0$ and such that

$$\tau = \begin{cases} 1, & \text{if } E > 0 \\ 0, & \text{elsewhere,} \end{cases} \tag{A7}$$

with $\rho^2 = 1 - \tau^2$. This energy step would naturally be implemented using a well-tuned electronic constriction, such as a quantum point contact [47]. The final expression for the scattering matrix of the whole system is as follows:

$$\begin{aligned} S &= \begin{pmatrix} r''_{11} & t''_{16} & t''_{17} \\ t''_{61} & r''_{66} & t''_{67} \\ t''_{71} & t''_{76} & r''_{77} \end{pmatrix} \\ &= \begin{pmatrix} \rho & i\tau t'_{16} & i\tau t'_{17} \\ i\tau t'_{61} & r'_{66} + t'_{61}\rho t'_{16} & t'_{67} + t_{61}\rho t'_{17} \\ i\tau t'_{71} & t'_{76} + t'_{71}\rho t'_{16} & r'_{77} + t_{71}\rho t'_{17} \end{pmatrix}. \end{aligned} \tag{A8}$$

It is worth observing that, having initialized all the $r_{pq}$ and $t_{pq}$ in Eq. (A1), the remaining (relevant) free parameters in the scattering matrix above are the difference between the paths in the upper/lower interference arms $\Delta L = L_+ - L_-$ and the magnetic flux enclosed in the interferometer loop $\Phi$ [see Eq. (A2)].

## APPENDIX B: CALCULATION OF THE ONSAGER COEFFICIENTS

We set, for simplicity, channel 7 (see Fig. 4) as the lead connected to the reference reservoir. Moreover, we set the relative dynamical phase $k\,\Delta L = \pi/2$ in order to maximize the effect of the sign flip of **B**. Using the Landauer-Büttiker formalism [48,49] and the scattering coefficients from Appendix A, we compute the Onsager coefficients,

$$\begin{aligned} L_{11} &= T \int dE(-\partial_E f)\tau^2, \\ L_{12} &= T \int dE\, E(-\partial_E f)\tau^2 = L_{21}, \\ L_{22} &= T \int dE\, E^2(-\partial_E f)\tau^2, \\ L_{33} &= T \int dE(-\partial_E f)\left[1 - \frac{1}{4}\cos^2\Phi(1+\rho)^2\right], \\ L_{34} &= T \int dE\, E(-\partial_E f)\left[1 - \frac{1}{4}\cos^2\Phi(1+\rho)^2\right] = L_{43}, \\ L_{44} &= T \int dE\, E^2(-\partial_E f)\left[1 - \frac{1}{4}\cos^2\Phi(1+\rho)^2\right], \\ L_{13} &= T \int dE(-\partial_E f)\left[-\frac{1}{2}\tau^2(1+\sin\Phi)\right], \\ L_{14} &= T \int dE\, E(-\partial_E f)\left[-\frac{1}{2}\tau^2(1+\sin\Phi)\right] = L_{23}, \\ L_{24} &= T \int dE\, E^2(-\partial_E f)\left[-\frac{1}{2}\tau^2(1+\sin\Phi)\right], \\ L_{31} &= T \int dE(-\partial_E f)\left[-\frac{1}{2}\tau^2(1-\sin\Phi)\right], \\ L_{41} &= T \int dE\, E(-\partial_E f)\left[-\frac{1}{2}\tau^2(1-\sin\Phi)\right] = L_{32}, \\ L_{42} &= T \int dE\, E^2(-\partial_E f)\left[-\frac{1}{2}\tau^2(1-\sin\Phi)\right], \end{aligned} \tag{B1}$$

where $f = [\exp\{E/k_BT\} + 1]^{-1}$ is the equilibrium Fermi distribution at temperature $T$ and $\mu = 0$.

[1] F. Giazotto, T. T. Heikkilä, A. Luukanen, A. M. Savin, and J. P. Pekola, Rev. Mod. Phys. **78**, 217 (2006).

[2] M. J. Martínez-Pérez, P. Solinas, and F. Giazotto, J. Low Temp. Phys. **175**, 813 (2014).

[3] G. J. Snyder and E. S. Toberer, Nature Mater. **7**, 105 (2008).

[4] A. Shakouri, Annu. Rev. Mater. Res. **41**, 399 (2011).

[5] Y. Dubi and M. Di Ventra, Rev. Mod. Phys. **83**, 131 (2011).

[6] G. Benenti, G. Casati, T. Prosen, and K. Saito, arXiv:1311.4430.

[7] A. N. Jordan, B. Sothmann, R. Sánchez, and M. Büttiker, Phys. Rev. B **87**, 075312 (2013).

[8] R. Sánchez, B. Sothmann, A. N. Jordan, and M. Büttiker, New J. Phys. **15**, 125001 (2013).

[9] B. Sothmann, R. Sánchez, and A. N. Jordan, Eur. Phys. Lett. **107**, 47003 (2014).

[10] N. Li, J. Ren, L. Wang, G. Zhang, P. Hänggi, and B. Li, Rev. Mod. Phys. **84**, 1045 (2012).

[11] V. Zhirnov, R. Cavin, and L. Gammaitoni, in *ICT-Energy-Concepts Towards Zero-Power Information and Communication Technology*, edited by G. Fagas, L. Gammaitoni, D. Paul, and G. A. Berini (InTech, Rijeka, Croatia, 2014).

[12] M. Terraneo, M. Peyrard, and G. Casati, Phys. Rev. Lett. **88**, 094302 (2002).

[13] B. Li, L. Wang, and G. Casati, Appl. Phys. Lett. **88**, 143501 (2006).

[14] C. W. Chang, D. Okawa, A. Majumdar, and A. Zettl, Science **314**, 1121 (2006).

[15] W. Kobayashi, Y. Teraoka, and I. Terasaki, Appl. Phys. Lett. **95**, 171905 (2009).

[16] H. Tian, D. Xie, Y. Yang, T.-L. Ren, G. Zhang, Y.-F. Wang, C.-J. Zhou, P.-G. Peng, L.-G. Wang, and L.-T. Liu, Sci. Rep. **2**, 523 (2012).

[17] O.-P. Saira, M. Meschke, F. Giazotto, A. M. Savin, M. Möttönen, and J. P. Pekola, Phys. Rev. Lett. **99**, 027203 (2007).

[18] R. Scheibner, M. König, D. Reuter, A. D. Wieck, C. Gould, H. Buhmann, and L. W. Molenkamp, New J. Phys. **10**, 083016 (2008).

[19] M. J. Martínez-Pérez, A. Fornieri, and F. Giazotto, Nat. Nanotechnol. **10**, 303 (2015).

[20] Z. Chen, C. Wong, S. Lubner, S. Yee, J. Miller, W. Jang, C. Hardin, A. Fong, J. E. Garay, and C. Dames, Nat. Commun. **5**, 5446 (2014).

[21] R. Sánchez, B. Sothmann, and A. N. Jordan, Phys. Rev. Lett. **114**, 146801 (2015).

[22] R. Sánchez, B. Sothmann, and A. N. Jordan, arXiv:1503.02926.

[23] G. Benenti, K. Saito, and G. Casati, Phys. Rev. Lett. **106**, 230602 (2011).

[24] K. Saito, G. Benenti, G. Casati, and T. Prozen, Phys. Rev. B **84**, 201306(R) (2011).

[25] V. Balachandran, G. Benenti, and G. Casati, Phys. Rev. B **87**, 165419 (2013).

[26] K. Brandner, K. Saito, and U. Seifert, Phys. Rev. Lett. **110**, 070603 (2013).

[27] K. Brandner and U. Seifert, New J. Phys. **15**, 105003 (2013).

[28] C. Blanc, A. Rajabpour, S. Volz, T. Fournier, and O. Bourgeois, Appl. Phys. Lett. **103**, 043109 (2013).

[29] T. Meier, F. Menges, P. Nirmalraj, H. Hölscher, H. Riel, and B. Gotsmann, Phys. Rev. Lett. **113**, 060801 (2014).

[30] Y. Ji, Y. Chung, D. Sprinzak, M. Heiblum, D. Mahalu, and H. Shtrikman, Nature **422**, 415 (2003).

[31] I. Neder, M. Heiblum, Y. Levinson, D. Mahalu, and V. Umansky, Phys. Rev. Lett. **96**, 016804 (2006).

[32] I. Neder, N. Ofek, Y. Chung, M. Heiblum, D. Mahalu, and V. Umansky, Nature (London) **448**, 333 (2007).

[33] P. Roulleau, F. Portier, D. C. Glattli, P. Roche, A. Cavanna, G. Faini, U. Gennser, and D. Mailly, Phys. Rev. B **76**, 161309(R) (2007).

[34] V. Giovannetti, F. Taddei, D. Frustaglia, and R. Fazio, Phys. Rev. B **77**, 155320 (2008).

[35] E. V. Deviatov and A. Lorke, Phys. Rev. B **77**, 161302(R) (2008).

[36] C. Altimiras, H. le Sueur, U. Gennser, A. Cavanna, D. Mailly, and F. Pierre, Nat. Phys. **6**, 34 (2010).

[37] P. P. Hofer and B. Sothmann, arXiv:1502.04920.

[38] H. B. Callen, *Thermodynamics and an Introduction to Thermostatics*, 2nd. ed. (Wiley, New York, 1985).

[39] The only limitation being not to set all of the $\{X_k^T\}$'s to be null: This configuration in fact only admits $\{X_k^\mu\} = 0\ \forall\ k$, hence no currents would flow through the device. In this scenario the $\{X_k^\mu\}$'s become explicit functions of the temperatures $\{X_k^T\}$ and of the Onsager coefficients $L_{ij}$.

[40] We want to stress that all our analysis is performed in the linear-response regime, therefore the allowed values of the currents are always limited by this approximation.

[41] Note, however, that in general the entropy production rate is nonzero due to the irreversible component of the particle current.

[42] S. Datta, *Electronic Transport in Mesoscopic Systems* (Cambridge University Press, Cambridge, UK, 1995).

[43] F. Mazza, R. Bosisio, G. Benenti, V. Giovannetti, R. Fazio, and F. Taddei, New J. Phys. **16**, 085001 (2014).

[44] We have used the fact that due to the symmetries of the scattering matrix, the Onsager matrix is block diagonal, and therefore $L_{21} = L_{12}$ and $L_{43} = L_{34}$.

[45] O. Entin-Wohlman, Y. Imry, and A. Aharony, Phys. Rev. B **91**, 054302 (2015).

[46] O. Entin-Wohlman and A. Aharony, Phys. Rev. B **85**, 085401 (2012).

[47] H. van Houten, C. W. J. Beenakker, and B. J. van Wees, in *Nanostructured Systems*, Semiconductors and Semimetals, edited by M. Reed, Vol. 35 (Academic Press, Boston, 1992), pp. 9–112.

[48] R. Landauer, IBM J. Res. Dev. **1**, 223 (1957).

[49] M. Büttiker, Phys. Rev. Lett. **57**, 1761 (1986).